A coupled mode model for omnidirectional three-dimensional underwater sound propagation

Brendan J. DeCourcy, and Timothy F. Duda

Citation: The Journal of the Acoustical Society of America **148**, 51 (2020); doi: 10.1121/10.0001517
View online: https://doi.org/10.1121/10.0001517
View Table of Contents: https://asa.scitation.org/toc/jas/148/1
Published by the Acoustical Society of America

JASA ARTICLE

A coupled mode model for omnidirectional three-dimensional underwater sound propagation

Brendan J. DeCourcy[a] and Timothy F. Duda
Applied Ocean Physics and Engineering, Woods Hole Oceanographic Institution, Woods Hole, Massachusetts 02543, USA

ABSTRACT:
A fully three-dimensional (3D) omnidirectional numerical coupled mode model of acoustic propagation is detailed. A combination of normal mode and finite element computational methods is applied to produce the numerical results. The technique is tested in a strongly range-dependent ocean environment modeled after the Hudson Canyon. Modeled sound from three source locations selected over different bathymetric depths is examined to determine capabilities and difficulties associated with varying numbers of propagating vertical modes across the horizontal domain, and variable amounts of mode coupling. Model results are compared to those from a unidirectional Cartesian 3D parabolic equation simulation, and from adiabatic (uncoupled) simulations to illustrate the capabilities of the techniques to study the influences of coupling, strong refraction, and reflection.
 https://doi.org/10.1121/10.0001517

(Received 15 January 2020; revised 4 June 2020; accepted 15 June 2020; published online 7 July 2020)

[Editor: D. Benjamin Reeder] Pages: 51–62

I. INTRODUCTION

Sound propagation in and around strongly range variable ocean regions presents a complex set of issues for numerical modeling and acoustic field prediction efforts. The four-dimensional acoustic wave equation, reduced to the three-dimensional (3D) Helmholtz equation by an assumption of a single frequency sound source, cannot be cleanly separated with respect to standard coordinates in a realistic environment; perhaps fundamentally, the boundary conditions are not applied parallel to coordinate unit vectors. Furthermore, the quantity of discrete grid points needed to produce a numerically stable omnidirectional 3D solution that includes propagation and scattering in all directions produces a high computational cost which increases with sound frequency. Despite the difficulty of this problem, a wealth of scientific work has produced many useful methods of estimating acoustic propagation in realistic environments. These methods, however, invariably require approximations of the acoustic and material physics which may limit their applicability in some circumstances.

Although a perfect separation of variables is impossible in any topographically realistic ocean environment, a common method of approximating the solution of the 3D Helmholtz equation is the method of normal modes.[1,2] This method separates the time-independent pressure $p(x, y, z)$ into vertical modes and their range-dependent amplitudes.[3,4] Furthermore, the range-dependent nature of the normal modes encourages further approximation, as the resulting modal amplitude equations are coupled.[5–7] To avoid the difficulties inherent in handling mode coupling and to make higher source frequency computations easier, ray theory[8] and beam-tracing have been used.[9] The ray and beam methodologies inherently include omnidirectional wave propagation in three dimensions which is a strength of these methods, but their applicability is limited in cases of low frequency or instances with surface ducts.[9] Another popular acoustic calculation approach is the Parabolic Equation (PE) method.[10,11] The fundamental PE approach increases numerical efficiency by including only the forward-propagating portion of the acoustic field, clearly excluding many propagation and scattering effects. While two-way PE variants do exist, these are largely restricted to idealized propagation environments.[13,14]

This paper will present a fully omnidirectional 3D acoustic propagation model based on extensions of previous work in normal mode[3,12] and mode coupling theories.[6,7] To test the effects of range-variable environments on acoustic propagation, the method is used to compute acoustic fields in a model of the Hudson Canyon which lies on the New Jersey Shelf Break and has already been the subject of acoustic study.[15] A discussion of the techniques used is given, and a sampling of numerical results which illustrate the influence of strongly variable canyon bathymetry on acoustic propagation are presented.

II. THEORETICAL FORMULATION

In the work described here, the approach taken is a reformulation of Fawcett's[7] two-dimensional (2D, one vertical, one horizontal coordinate) mode coupling derivations to extend them to a 3D domain. Here, the ocean environment is described by Cartesian coordinates (x, y, z), with z being the vertical coordinate, with the ocean surface located at $z = 0$, and the bottom located at $z = b(x, y) < 0$. The starting point is the 3D Helmholtz equation for acoustic pressure

[a]Electronic mail: bdecourcy@whoi.edu, ORCID: 0000-0003-0978-5791.

$p(x,y,z)$ from a constant frequency f acoustic point source at (x_s,y_s,z_s) in a medium with sound speed $c(x,y,z)$ and acoustic wavenumber $k(x,y,z)=2\pi f/c$. A modal decomposition of p is given by

$$p(x,y,z)=\sum_{n=1}^{\infty}R_n(x,y)\phi_n(z|x,y), \tag{1}$$

where n represents the vertical mode number, ϕ_n are orthonormal vertical modes which satisfy locally flat-bottom impedance conditions at $z=b(x,y)$, and R_n are the modal amplitudes. The vertical mode functions ϕ_n are solved for a locally Pekeris-type vertical waveguide, comprised of a variable water column and a half-space for the ocean bottom using the ORCA normal mode program.[12] Following Fawcett's method, a coupled equation for the vertical mode amplitudes is derived:

$$\nabla_h^2 R_n + K_n R_n = -\sum\nolimits_{m\neq n}[\underline{\mathbf{B}}_{nm}\cdot\nabla_h R_m + A_{nm}R_m] - \frac{4\pi}{\rho_w}\phi_n(z_s|x,y)\delta(x-x_s)\delta(y-y_s), \tag{2}$$

where ∇_h^2 is the horizontal Laplacian differential operator in (x,y), $K_n=k_{h,n}^2+A_{nn}$, $k_{h,n}$ is the horizontal wavenumber of mode n, $\underline{\mathbf{B}}_{nm}$ and A_{nm} are coupling coefficients, and ρ_w is the density of the ocean water. The coupling coefficients are derived by Fawcett[7] for 2D acoustic propagation, and in three dimensions are given by

$$\underline{\mathbf{B}}_{nm}=2\int_{-\infty}^{0}\frac{1}{\rho}(\nabla_h\phi_m)\phi_n dz - \nabla_h b\left(\frac{1}{\rho_w}-\frac{1}{\rho_b}\right)(\phi_m\phi_n)_{z=b}, \tag{3}$$

$$A_{nm}=\int_{-\infty}^{0}\frac{1}{\rho}(\nabla_h^2\phi_m)\phi_n dz - \nabla_h b\cdot\left[\frac{1}{\rho}\nabla_h\phi_m\right]_{z=b}\phi_n|_{z=b}, \tag{4}$$

where the integrals represent a transfer of energy between modes due to horizontal changes to the water column such as sound speed fronts, or changing water depth. In these equations, the notation $\lceil\cdot\rceil_{z-b}=\lceil\cdot\rceil_{z-b^-}-\lceil\cdot\rceil_{z-b^+}$ is a difference between functional values on either side of the water/bottom interface, and the subscript $z=b$ simply means evaluation at $z=b$. The second term in each coupling coefficient is proportional to $\nabla_h b$ and accounts for the coupling influence of the bottom slope which is lost in the flat-bottom impedance conditions applied to ϕ_n.

One strength of this formulation of the coupling coefficients is that it clearly separates the influence of flat-bottom vertical modes which can be computed without knowing the local bathymetric slope, and the influence of the slope itself. To examine the influence of local bathymetric slope (here defined as the actual slope of the bottom at a discrete position in a horizontal numerical grid) compared to a smoother approximation of bathymetric slope (implicitly defined by the variable bathymetry depths and represented by a centered difference approximation), one could compare the relative sizes of the two components of each coupling coefficient. Letting $\nabla_h b=\nabla_h\tilde{b}+\underline{\beta}$ where $\nabla_h\tilde{b}$ represents the numerical centered difference approximation for bathymetric slope and $\underline{\beta}$ is a perturbation representing the uncertainty of local slopes, some analyses can be carried out to probe the sensitivity of acoustic fields to local slopes on the bathymetry grid, but this does not fall within the scope of this paper.

A reasonable approximation can be computed by limiting the number of modes used to only include those that propagate as well as a finite selection of leaky modes to approximate the near field and seabed sound penetration at sloped seabed locations, and then solving for all R_n simultaneously. In three dimensions, however, the amount of computational power required to handle a typical horizontal domain is incredibly large. Additionally, the concept of computing the coupling coefficients and necessary horizontal derivatives of vertical modes requires careful treatment to deal with the strongly range-dependent water/bottom interface and the integration of leaky modes. These issues will be considered in Secs. III and IV.

III. HORIZONTAL DIFFERENTIATION OF THE VERTICAL MODES

Horizontal differentiation of the vertical mode functions ϕ_n and the bathymetry function b appear in both coupling coefficients given by Eqs. (3) and (4). For the numerical implementation, these derivatives must be approximated in a way that preserves some level of numerical accuracy that is acceptable for the model. The horizontal gradient of the bathymetry function $\nabla_h b$ is a measurement of the local slopes, but for a realistically rough water/bottom interface it is not reasonable to expect that the precise slope or even a close approximation can be obtained at all desired locations. Therefore, a convenient centered difference approximation which is accurate to $O(h^2)$ for grid spacing h on a uniform grid can be used for bottom slope calculations. If a finer sampling of bottom slope is needed, a linear interpolation of the centered difference slope approximations will imply a smoothly varying bottom. It is important to note that differences in bottom slope representation can influence acoustic field effects,[16] but because the bottom slope cannot be known precisely at all locations in a realistic environment, this issue will not be addressed here.

Differentiation of the vertical modes raises its own issues. Primarily, the question of how to numerically handle horizontal derivatives near the water/bottom interface arises. The vertical modes are by design vertically differentiable; near interfaces a one-sided three-point finite difference scheme can give a second-order accurate approximation of the first derivative, and the interface conditions can be used to estimate the value of $\partial\phi_n/\partial z$ at the interface. However, horizontal differentiation runs into the issue of needing to

https://doi.org/10.1121/10.0001517

incorporate carefully crafted differentiation schemes designed to handle the generally off-grid water/bottom interface, across which the vertical mode derivatives are discontinuous in z. An alternative approach is to replace z with bottom-following sigma coordinates often used in meteorological and oceanographic contexts,[17,18] and directional derivatives along sigma surfaces can be used to compute the horizontal derivatives.

The sigma coordinates will be defined differently depending on whether they represent data in the water or the bottom. In the water, the coordinate $\sigma_w = b_0(z/b)$ defined for a water/bottom interface at $z = b(x, y)$ and reference water depth b_0 conserves the ratio of z to $b - z$ along surfaces of constant σ_w. In the bottom, the coordinate $\sigma_b = H - (H - b_0)(H - z)/(H - b)$ for some $|H| \gg |b|$ with $H < 0$ conserving the ratio of $z - b$ to $H - z$ along constant σ_b. In a fixed vertical plane such as $y = y_p$, the unit vector

$$\vec{\nu} = (\nu_1, \nu_2) \equiv \frac{\left(\partial_z \sigma(y_p), -\partial_x \sigma(y_p)\right)}{\sqrt{\left(\partial_x \sigma(y_p)\right)^2 + \left(\partial_z \sigma(y_p)\right)^2}} \tag{5}$$

lies along a curve of constant $\sigma(y_p)$, and the directional derivative along this curve is given by $D_{\vec{\nu}}\phi_n = \nu_1 \phi_{n,x} + \nu_2 \phi_{n,z}$. A numerical approximation of $D_{\vec{\nu}}\phi_n$ can be computed by interpolating the function ϕ_n to the σ depth grid, computing a standard finite difference approximation on the new data, and interpolating back to the initial z grid. In this way, derivatives $\phi_{n,x}$ and $\phi_{n,y}$ can be approximated smoothly without crossing the water/bottom interface, by solving for $D_{\vec{\nu}}\phi_n$ and $\phi_{n,z}$ first, and using the directional derivative formula to find the horizontal derivatives.

The integrals in Eqs. (3) and (4) can be computed numerically using a fine z grid, and using the interface conditions on ϕ_n at $z = b$. The integrals are approximated by using a depth grid that truncates at $z = H \ll b$, as defined for the bottom sigma coordinate. This H value is chosen such that the selections of normal modes used in the computation have all decayed to a pre-selected numerically insignificant value. Furthermore, in order to handle the transition from deeper water to shallow regions, a small attenuation and sound speed gradient is inserted into the bottom following the method of Westwood and Koch.[3] This forces leaky modes to eventually decay and become integrable,[3,19] as without the gradient the amplitude of the leaky vertical modes grows exponentially. By including some of the leaky modes, the leading order effects of coupling into lossy modes at the slopes are included.

As will be noted in Sec. IV, there is a difference in the grid density requirements for horizontal differentiation of the bathymetry or vertical mode data, and requirements to resolve oscillations of the mode amplitudes, with the latter demanding a much finer grid. Since the differences in ϕ_n from one horizontal position to another derive from changes to the water column between the two locations, and because the intervening values cannot be known precisely for a realistic environment, interpolation of data from a coarse grid for $\underline{\mathbf{B}}_{nm}$ and A_{nm} is acceptable, given that the grid is dense enough to resolve the local characteristics of range dependence. For this work, the bathymetry is considered the primary cause of vertical waveguide variation, so a grid spacing derived from the bathymetry variation is proposed for evaluating the coupling coefficients. A convenient method to define a bathymetrically sensitive coarse grid is to require that the inequality $|b| \gg |\Delta x b_x|$ is satisfied for grid spacing Δx, and likewise for the y direction. Given two adjacent values of b on a grid in x defined as $b_{i+1} = b(x_{i+1})$ and $b_i = b(x_i)$, the grid spacing is chosen such that

$$2\left|\frac{b_{i+1} - b_i}{b_{i+1} + b_i}\right| \leq \epsilon, \tag{6}$$

for some $\epsilon \ll 1$. This discretization of $|b| \gg |\Delta x b_x|$ uses a centered difference approximation for the derivative and an average value of b over the interval x_i to x_{i+1}. If new points are needed to fill in gaps in the user supplied grid either at this step or later, interpolation will be used to supply needed information. A differentiable interpolation method is desired, and in this case the "makima" or "modified Akima" method supplied by MATLAB was used. This method is also used to horizontally interpolate the mode functions expressed vertically in the bottom following sigma coordinates in Eq. (5).

IV. SOLVING THE 2D HELMHOLTZ EQUATION

The most challenging aspect of the numerical implementation of this method is solving the mode amplitudes defined by Eqs. (2)–(4). Due to Eq. (2) being coupled, in order to avoid the need to solve for each mode coefficient simultaneously, it must first be de-coupled. One approach is to begin by replacing the coupling term in Eq. (2) with an estimate based on approximations of the mode coefficients, and converging to a numerically exact solution through an iterative process.[6] To do so, the mode amplitude equation is first expressed as

$$\nabla_h^2 R_n + K_n R_n = -S_{n,0} - S_{n,C}(R), \tag{7}$$

where $S_{n,0} = 4\pi\rho_w^{-1}\phi_n(z_s|x, y)\delta(x - x_s)\delta(y - y_s)$ is the point source term, and $S_{n,C}(R)$ is the remaining sum on the right side of Eq. (2). The adiabatic approximation to Eq. (7) assumes no coupling, and is the solution to case $S_{n,C} = 0$. This equation can be solved individually for each mode. Using the adiabatic $R_n^{(0)}$ as an initial approximation for the mode coefficients, an iterative equation to approximate R_n is given by

$$\nabla_h^2 R_n^{(j+1)} + K_n R_n^{(j+1)} = -S_{n,0} - S_{n,C}(R^{(j)}), \tag{8}$$

with a relative error estimate for $R_n^{(j+1)}$ given by

$$E_{j+1} = 2\frac{|S_{n,C}(R^{(j+1)})| - |S_{n,C}(R^{(j)})|}{|S_{n,C}(R^{(j+1)})| + |S_{n,C}(R^{(j)})|}. \tag{9}$$

The iterative refinement process can be continued until E_{j+1} is sufficiently small on a sufficiently large percentage of the horizontal domain. For the purposes of this paper, the *ad hoc* restriction chosen is that less than 50 square meters of the domain excluding the sponge region has greater than a 1% error as measured by Eq. (9).

Now that the mode equations have been de-coupled they must be solved numerically. A finite element approach can be used, which has the benefit of being able to handle a point source $S_{n,0}$ as well as a nontrivial coupling term $S_{n,C}$ throughout the horizontal domain. Transition to a weak formulation of the problem follows the standard method of multiplying Eq. (8) by a test function and integrating over the horizontal domain.[20] This domain is described by a uniform square grid with grid spacing of ten points per horizontal modal wavelength. To address the boundary conditions, an artificial absorbing sponge layer is placed on the edges of the domain to eliminate boundary reflections and emulate an outward radiation condition.[21] Due to the sponge layer, boundary integrals reduce to zero. Numerical convergence of the Helmholtz equation solution was confirmed by comparing computed solutions to $\nabla_h^2 u + k^2 u = -\delta(x)(y)$, to the analytical Green's function solution $u_g(x,y) = -(i/4)H_0^{(1)}(kr)$, with $r = \sqrt{x^2+y^2}$ and fixed $k = 2\pi/30$. Calculating the numerical solution on a grid with spacing $h_1 = \lambda/10$ and $h_2 = \lambda/20$ with $\lambda = 2\pi/k$, and then comparing the errors $\xi_1 = u_1 - u_g$ and $\xi_2 = u_2 - u_g$, where u_j is computed on the numerical grid with spacing h_j, the convergence rate of the method can be estimated. Along the curve $x = 1750$, $-250 < y < 250$ measured in meters, the error is assumed to take the form $E_j \approx Ch_j^{\mu}$, such that $\mu \approx \log(|\xi_1|/|\xi_2|)/\log(2)$. The mean value of μ is computed to be $\mu = 1.947 \pm 0.009$, with the uncertainty listed spanning one standard deviation above and below the mean value. This is consistent with a numerical scheme with accuracy to $O(k^2h^2)$. A similar comparison between the h_1 grid and a $h_4 = \lambda/40$ computation yields an μ estimate of $\mu = 1.969 \pm 0.005$. The accuracy tests reveal phase lags in the computed modal waves that grow with range from the source even when the amplitude remains accurate. This phase lag is proportional to $\nu(kh)^2 r$, where r is the distance from the source, k is the horizontal wavenumber, h is the grid spacing, and ν is a small constant which has been calculated to be approximately $\nu \approx 0.0075$. Phase lag in finite element solutions to the Helmholtz equation have been studied,[22] and this is an acknowledged difficulty of the method which can be addressed when needed by reducing h.

V. TEST OF REFLECTION AND REFRACTION

In the adiabatic approximation, the coupling coefficients $\vec{B}_{nm}$ and A_{nm} which incorporate the bottom slope influence are set to zero, so some of the physics of bottom reflection is lost. To illustrate how this affects simulations, a simple example of a Pekeris type waveguide with a reflecting berm is examined. Consider a 100 m deep waveguide with a homogeneous 1500 m/s sound speed ocean over a 2000 m/s sound speed bottom with density 1.9 g/cm^3 and attenuation 0.8 dB per acoustic wavelength. A 30 m high berm is added, with the seabed otherwise flat. The berm crest is parallel to the y axis and the berm has no y dependence.

Figure 1(a) shows the bathymetry in this model. The berm begins at $x = 1100$, plateaus between $x = 1160$ and 1170, and slopes downward again until $x = 1230$. The wall sides have a slope of approximately 26.565 degrees.

To examine the influence of reflection and refraction that is captured by the adiabatic and coupled mode theories, the model is run for three cases, all with a 50 Hz sound source: with no berm, with the berm and no coupling, and with the berm and coupling. Six modes are computed for a point source of 50 Hz placed at $x = 400$ and $z = 5$ m. For reference, the real portions of the horizontal modal wavenumbers are shown in Fig. 1(b), with the thick dashed line representing the wavenumber in the bottom, such that modes falling below this line are expected to attenuate strongly horizontally. The vertical dashed lines represent the beginning and end of the berm. Mode 1 appears at the top of the figure, with mode 6 as the bottom curve.

Let the outgoing acoustic pressure field which is calculated with no berm be given by p_O, the incoming field from the adiabatic approximation be given by $p_{S,A} = p_A - p_O$, and coupled given by $p_{S,C} = p_C - p_O$, where p_A and p_C are the adiabatic and coupled pressure fields. Figures 2(a) and 2(d) show the intensity and phase associated with p_O at a depth of $z = 30$ m, given by $20\log_{10}|p_O|$ and $\arg(p_O)$, while Figs. 2(b) and 2(e) show the same for $p_{S,A}$, and Figs. 2(c) and 2(f) show $p_{S,C}$. Examining the results, it is evident that the coupled mode approximation captures 10 to 20 dB more scattered sound than the adiabatic approach on the source side of the berm. On the opposite side a higher amount of energy is scattered with the coupled approximation as well, this time from a combination of energy bouncing off the berm in a forward manner, and the absence of energy that is scattered back toward the source. A similar representation of outgoing and scattered sound is given in Fig. 3, where only mode 3 is illustrated. In this instance the difference between adiabatic and coupled scattering is quite stark on the source side of the berm, where very little sound is reflected backwards. All of this goes to show that while the adiabatic approximation can certainly account for some acoustic reflection and refraction from sloping bottoms, the coupled mode method is absolutely necessary to account for a more complete physical representation of the acoustics. In particular, the adiabatic scattered field shows little or no reflection of sound that encounters the berm at normal incidence, although it does show some energy that has refracted while encountering the berm at non-normal incidence.

For an additional test of the method accuracy, the adiabatic approximation field can be benchmarked by comparing the energy that is scattered due to a single abrupt "step" change in the bathymetry, to a reflection coefficient estimate using vertically homogeneous layers in the ocean and Rayleigh reflection coefficients at layer interfaces. Consider

https://doi.org/10.1121/10.0001517

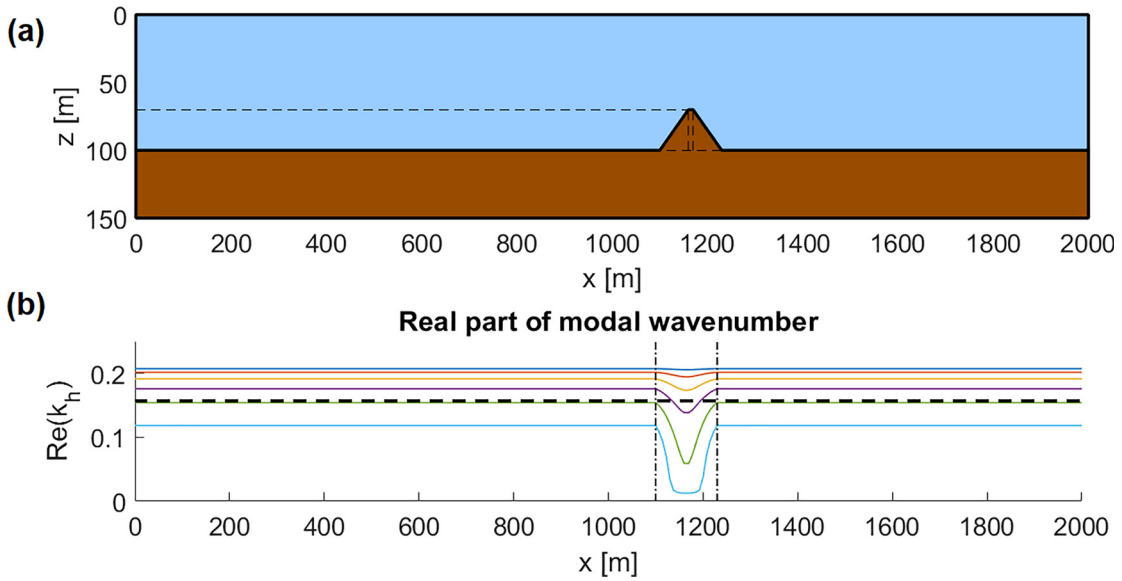

FIG. 1. (Color online) (a) Bathymetry for the simple berm model. The top (blue) layer represents 1500 m/s water, while the bottom (brown) layer represents 2000 m/s sediment, with a bottom density of 1.9 g/cm^3, and attenuation of 0.8 dB/acoustic wavelength. The bathymetry is composed of straight lines connecting the (x, z) pairs: (0, 100), (1100, 100), (1160, 70), (1170, 70), (1230, 100), (2000, 100). Horizontal dashed lines are inserted for perspective relative to vertical axis. Vertical dashed lines indicate the flat top of the berm. (b) Real components of the horizontal wavenumbers $\mathrm{Re}(k_{h,n})$, for modes $n = 1$ through 6. The horizontal dashed line is at $k_b = 2\pi f/c_b \approx 0.157$ m^{-1}, being the wavenumber in the bottom. Vertical dashed lines indicate the beginning and end of the berm. Mode 1 is the top-most curve, counting down to mode 6 as the bottom-most curve.

a 100 m deep waveguide with a constant sound speed containing one 50 Hz source, which transitions to a 75 m deep waveguide over the short distance of 5 m (1/6th of a wavelength in the 1500 m/s ocean), and lies above a bottom identical to that of the berm model. Reusing the berm notation, the unperturbed pressure in a homogeneous 100 m deep waveguide is given by p_O and is the outgoing field. The scattered portion of the adiabatic approximation for the step waveguide is given by $p_A - p_O$, where p_A is the adiabatic approximation in the step waveguide. For each mode, the amplitude is expressed similarly as $R_{O,m}$ for the amplitude of the outgoing mode m, and $R_{A,m} - R_{O,m}$ for the amplitude of the scattered portion of mode m. Then the difference in intensity of each mode at the step is evaluated as $\mathrm{REF}_A = 20\log_{10}(|R_{A,m} - R_{O,m}|/|R_{O,m}|)$. A second estimate for the scattered sound at the step is given by evaluating the influence of horizontal reflection coefficient across the step, as $\mathrm{REF}_T = 20\log_{10}(|k_{75} - k_{100}|/|k_{75} + k_{100}|)$, where k_{75} and k_{100} are the horizontal wavenumbers on the 75 and 100 m sides of the step. A comparison of these results is given in Table I.

While not a perfect match, the small differences in the two estimates can be, in part, explained by the step not being truly instantaneous, and the implied approximation that each

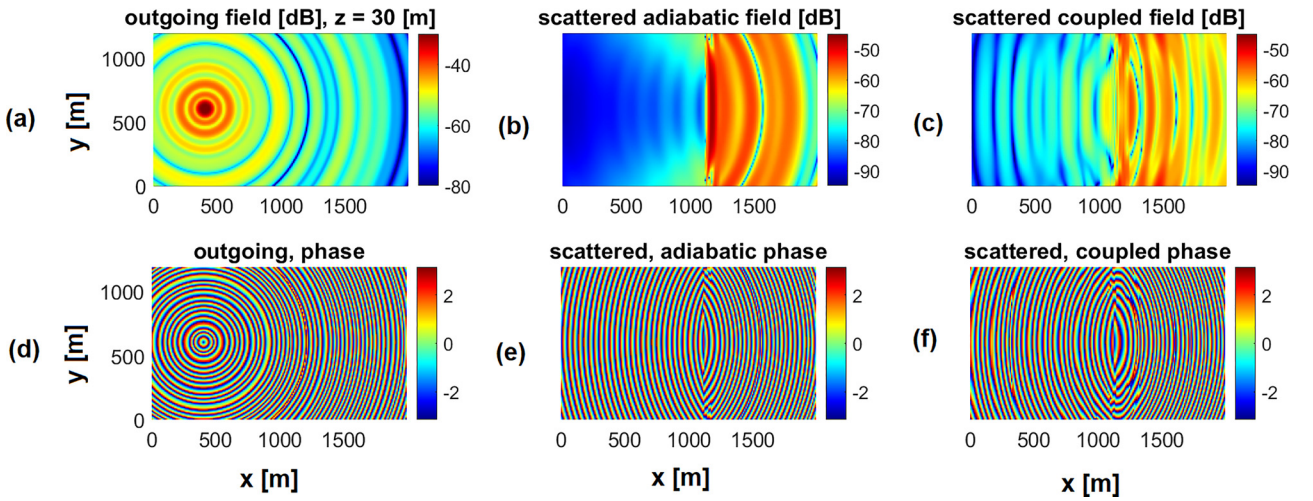

FIG. 2. (Color online) Output from calculations from the flat-bottom and berm environments are shown at a depth of $z = 30$ m. (a) The flat-bottomed (p_O) result is shown, which has only outgoing sound. (b) The dB scale difference between the adiabatic berm result ($p_{S,A}$) and the flat bottom result is shown, which is the berm-scattered field. (c) The dB scale difference between the coupled berm result ($p_{S,C}$) and the flat bottom result is shown. (d), (e), and (f) are the phases for the cases shown in (a), (b), and (c), respectively.

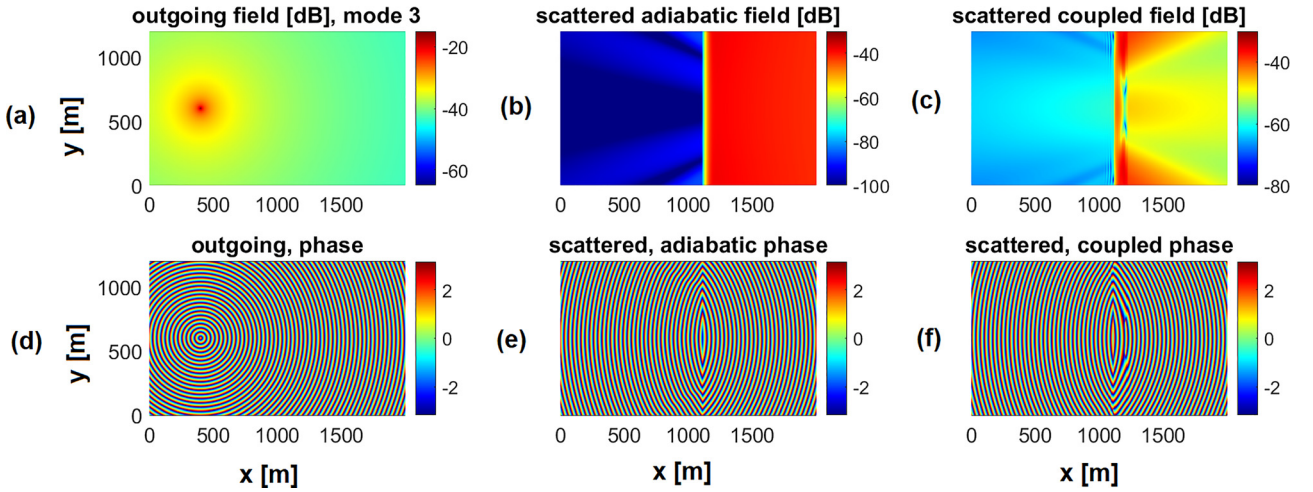

FIG. 3. (Color online) Comparison of adiabatic and coupled models for vertical mode 3 in the berm model. Subfigures (a), (b), and (c) represent outgoing, adiabatic scattered, and coupled scattered dB scale mode 3 amplitudes, while (d), (e), and (f) are the associated phases.

uses to handle this. While this does not benchmark the coupled mode output, it does show that in a simple step model, the adiabatic mode amplitude solution method is capable of producing good approximations.

VI. NUMERICAL OUTPUT

To test the method, a 9×14 km region of the upper Hudson Canyon is modeled. This region contains a variable bathymetry with water depths ranging from 81 to 494 m as shown in Fig. 4. Local bathymetric slopes in this domain range from nearly zero to 25 degrees and higher in some areas. In Fig. 4, the thick bathymetry levels denote 100, 200, 300, and 400 m depths, while the thin contours denote 50 m intervals, and the dashed contours are at 25 m intervals. The sound speed is given by a single profile for the water which is truncated at the water/bottom interface. As shown in Fig. 5, the sound speed is a downward refracting profile with a surface speed of 1536 m per second, and decreases to a minimum value of 1485 m per second. In Fig. 5, the horizontal line at 81 m represents the most shallow water measurement, while the horizontal line at 494 m is the deepest. The ocean floor is modeled as a sandy bottom, with a sound speed of 1650 m per second, density of 1.9 g per cubic centimeter, and attenuation of 0.8 dB per acoustic wavelength.

For the coupled mode output, the process for choosing the number of modes to include is not trivial. The propagating modes as well as a finite number of leaky modes must be included to approximate the field near the source.[16] In the case of a fully reflecting seabed, the number of required modes would be straightforward to determine. Here, the number of water-trapped modes at the location where these are most numerous would be the minimum required, and improved simulation would result by adding a few modes that would be leaky everywhere. The presence of these leaky modes would change the results for energy transfer into the seabed at all coupling locations (sloped seabed locations). However, for an environment where sound penetrates the seabed such as used here, the mode set may transition

TABLE I. Step bathymetry test parameters.

Mode #	k_{100} [m^{-1}]	k_{75} [m^{-1}]	REF$_A$ [dB]	REF$_T$ [dB]
1	$0.2076 + i8 \times 10^{-6}$	$0.2064 + i2 \times 10^{-5}$	−50.7	−50.7
2	$0.2019 + i3 \times 10^{-5}$	$0.1966 + i6 \times 10^{-5}$	−37.6	−37.5
3	$0.1916 + i6 \times 10^{-5}$	$0.1783 + i0.0001$	−29.0	−28.9
4	$0.1760 + i0.0001$	$0.1495 + i0.0023$	−22.1	−21.8
5	$0.1543 + i0.0010$	$0.0921 + i0.0102$	−12.6	−11.9
6	$0.1185 + i0.0047$	$0.0142 + i0.0968$	−3.77	−1.56

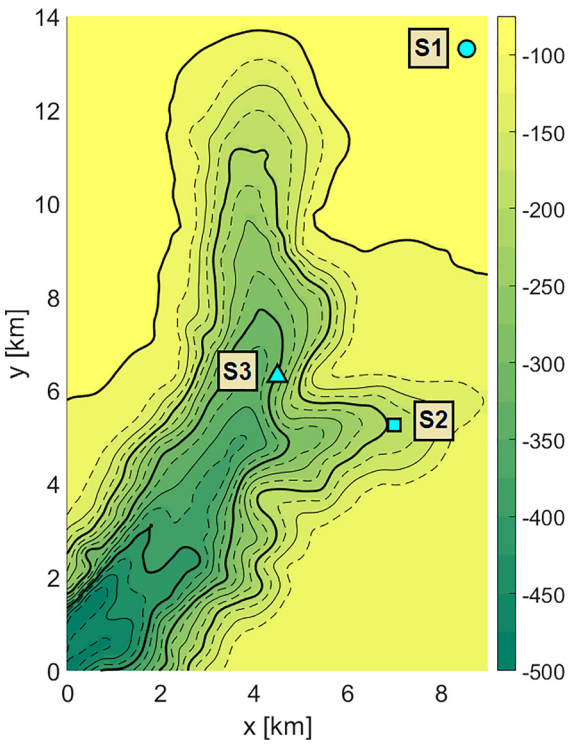

FIG. 4. (Color online) Hudson Canyon bathymetry. Markers represent locations of tested sound sources. Contours begin at 100 m depth and repeat at 25 m intervals. Sources are labeled S1, S2, and S3.

https://doi.org/10.1121/10.0001517

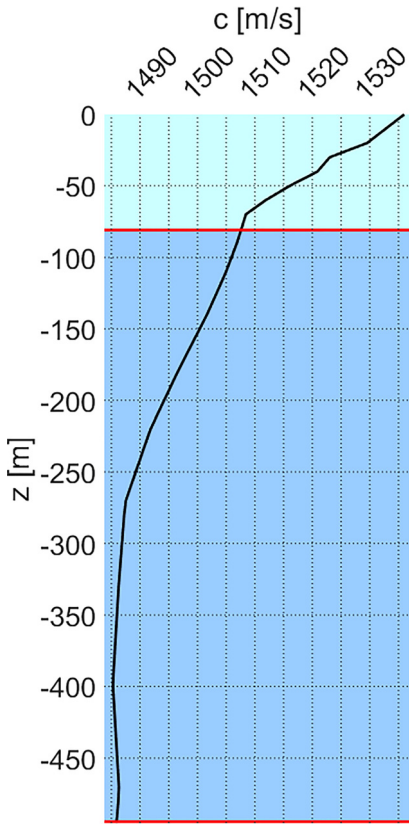

FIG. 5. (Color online) The depth-dependent sound speed in the water is plotted. The upper horizontal line (red) is at the most shallow water depth (81 m), bottom line (red) is at the deepest point (494 m).

gradually from fully trapped low-order modes (little or no attenuation) through slightly bottom interacting and slightly attenuating with range, to greatly attenuating, then to evanescent in the horizontal. In this case, the horizontal modal attenuation (the imaginary component of the horizontal modal wavenumber k_h[23]) provides an estimate of the horizontal range of influence of a given mode in the absence of coupling. In the adiabatic case, selecting modes which decay quickly within some selected distance from the source ensures that beyond that distance, the field is well approximated. However, with a strongly range-dependent environment where mode coupling is crucially important, propagating trapped modes can couple into strongly attenuating modes, increasing the horizontal area where these otherwise unimportant modes are energized, while also changing the energy content of the propagating modes (increasing bottom loss). Therefore, the simulated field will depend on the number of modes used. The coupling effects are difficult to know without actually completing the full calculation, which is not feasible in cases like the one presented here, where the computational demands can become large as the number of modes is increased. The number of modes used for these numerical examples was chosen by using a horizontal decay rate metric which is described in the following paragraph, including modes up to those with very strong horizontal attenuation, and then assessing the final coupled modal amplitudes to ensure that the highest mode included does exhibit strong range attenuation despite the coupling influence.

Mode amplitudes are proportional to $\exp(ik_h r)$, thus decay like $\exp(-\mathrm{Im}(k_h)r)$. The amplitude e-folding scale can be used as a decay metric,[24] i.e., $D = \mathrm{Im}(k_h)^{-1}$. In the cases tested here, 16 modes are included, with mode 16 having decay ranges of 2, 7, and 474 m at S1, S2, and S3, and mode 17 having decay ranges of 2, 6, and 381 m at S1, S2, and S3. Clearly, these are leaky modes at two of the source positions, and travel only a few wavelengths in the canyon at S3. With mode coupling, these ranges will no longer be accurate representations of the modal decay, but they are selected because of the high attenuation especially in the case of S1 and S2, and the coupled amplitude decay can be confirmed after computations are complete.

To examine how the coupled mode approach measures up to other propagation modeling methods, a 3D PE model was used to generate a comparison field.[10,11] For both models, a 50 Hz sound source is placed at a depth of 8 m over a 195 m deep location, which is marked by a square marker in Fig. 4. The intensity values for the modeled acoustic fields are plotted in dB on horizontal planes at depths of 9, 99, and 249 m for the coupled mode and PE models in Fig. 6. In these figures, black contours represent bathymetry depths on 50 m intervals starting with 100 m, and the dashed (blue) contours in Figs. 6(b) and 6(c) illustrate the water/bottom intersection for the plotted depth. A visual comparison of the two does reveal some shared behavior, but generally the field calculations represent quite different outcomes for interference patterns. The differences in interference patterns can be generally attributed to both a change in the propagation mechanisms being modeled (forward propagating PE, omnidirectionally propagating coupled modes, handling of bottom slope), and a known phase lag in the coupled mode model compared to unknown phase accuracy in the PE. This comparison aims to highlight the variations (or similarities) in model output, in the context of competing goals in acoustic modeling. Two goals in modeling acoustic propagation in a highly range-dependent environment include producing computationally efficient methods, and producing physically accurate outcomes. Both methods shown in Fig. 6 make physical and numerical approximations, and they do propagate comparable levels of acoustic energy especially along the x coordinate direction which is the propagation direction of the more computationally efficient PE. The importance of the coupled mode approach then is not simply in the ability to account fully for 3D effects of the omnidirectional acoustic propagation, but also that it provides a mechanism to study the transfer of modal energy that is represented by the modal coupling coefficients. While mode filtering can be used with PE output to study coupling effects, the coupling analysis cannot fully incorporate the out-of-plane effects as not all propagation directions are modeled. One potential use of the two models which has not been explored in this paper is that the presence of very high angle sound energy in the mode solution, not included in the PE solution, can be used to evaluate the

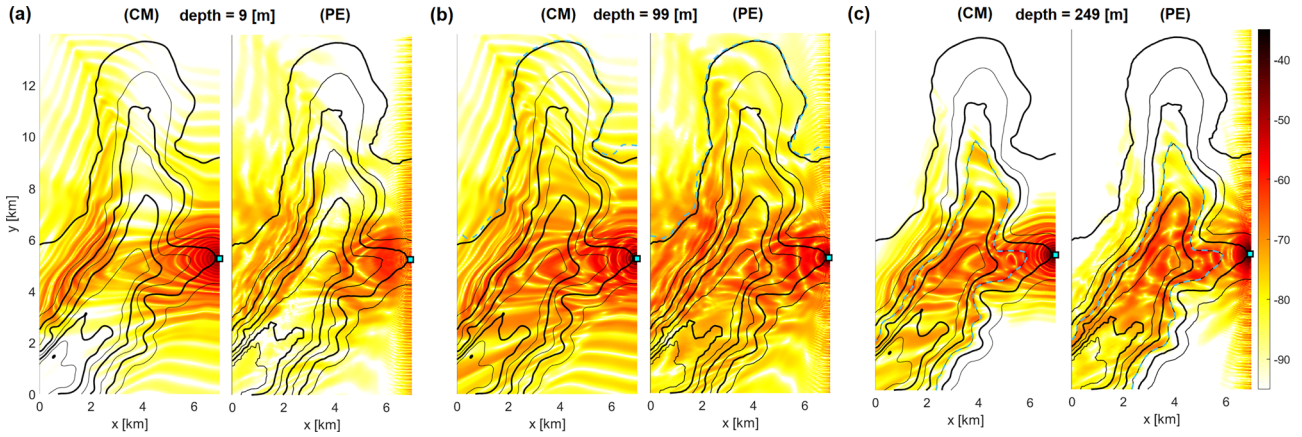

FIG. 6. (Color online) Horizontal plane slices of the transmission loss in the Coupled Mode (CM) and PE models are plotted for source S2 at a source depth of 8 m, with plane depths of 9 m in (a), 99 m in (b), and 249 m in (c). Thick contours represent bathymetry levels at 100 m intervals, beginning with 100 m. Thin contours represent bathymetry levels at 50 m intervals. The dashed (light blue) contours in (b) and (c) show the intersection of the plane with the water/bottom interface.

utility (or limitations) of the more practical PE, Gaussian beam, or forward-restricted coupled mode solutions in these challenging environments.

To illustrate the influence of the canyon on acoustic propagation, three separate sound sources are tested and acoustic fields are plotted on three horizontal planes. Source 1 (S1) is denoted by the circle marker in Fig. 4, and is at a depth of 8 m. The water depth at S1 is 89 m. Source 2 (S2) is denoted by the square marker in Fig. 4, and is the same source that generated Fig. 6. Like S1 it is located at a depth of 8 m, but here the water depth is 195 m. Source 3 (S3) is denoted by the triangle marker in Fig. 4, and is at a depth of 150 m where the total water depth is 297 m. The acoustic intensity in three horizontal planes at 8, 100, and 200 m deep is plotted for each source in Fig. 7, with the color levels matching those in Fig. 6.

In Figs. 7(a)–7(c) the influence of the canyon and the downward refracting sound speed profile on the field generated by S1 is clear. As the sound propagates over the canyon, it travels down from the surface toward the canyon floor, as evidenced by the relatively low intensity over the canyon at the 8 and 100 m levels, and the comparatively higher intensity in the 200 m plane. Similarly, S2 shown in Figs. 7(d)–7(f) exhibits the downward refracting influence of the sound speed profile, with acoustic energy propagating more strongly in the 200 m plane. Additionally, the focusing effect of the smaller arm of the canyon over which S2 is placed is clear, with the sound propagation being strongest along the thalweg of this part of the canyon. With S3 shown in Figs. 7(g)–7(i), the energy propagation is much stronger compared to S1 and S2, as more propagating modes exist deeper in the canyon, rather than decaying into the bottom.

To understand the importance of an omnidirectional propagation model in contrast to the forward propagation PE, consider some example modal amplitudes as shown in Figs. 8 and 9. Mode 8, illustrated in Fig. 8 over a more restricted 9 km × 9 km region, is the first mode that very clearly displays refraction/reflection from the canyon wall opposite the source location. For clarity, the dB scale magnitudes of the modes are shown. This is most clear in the adiabatic amplitude $10\log_{10}|R_8^{(0)}|^2$, but the coupled amplitude $10\log_{10}|R_8|^2$ is the more accurate representation of where vertical mode 8 propagates. Both adiabatic and coupled mode amplitudes show modal energy refracting/reflecting back from the canyon wall opposite the source location, which is behavior that cannot be fully captured in a forward-only propagation model. To clarify the importance of the coupling, a relative difference between adiabatic and coupled mode amplitudes is shown, where white indicates agreement in mode amplitude, while darker colors represent either stronger (red) or weaker (blue) propagation for the coupled amplitude compared with the adiabatic. The relative difference is computed as $\text{diff} = 2(\log_{10}|R_n| - \log_{10}|R_n^{(0)}|)/(\log_{10}|R_n| + \log_{10}|R_n^{(0)}|)$, similar to the relative difference calculation in Eq. (9). At points where both $-20\log_{10}|R_n| > 120$ and $-20\log_{10}|R_n^{(0)}| > 120$, the relative difference calculation is forced to be zero, with the intention of de-emphasizing the difference at locations where both the adiabatic and coupled mode amplitudes exhibit high energy loss. This also eliminates the numerical issues associated with the relative difference metric in the case where both amplitudes equal zero. Figure 9 similarly presents the adiabatic and coupled amplitudes for mode 11, and their relative difference.

In Figs. 8 and 9, the adiabatic mode amplitudes cannot show explicit horizontal reflection from the changing bathymetry, which is contained within the mode coupling coefficients in Eqs. (3) and (4). The coupled mode amplitudes do contain both vertical and horizontal reflection information. In both situations, strong refraction and reflection show that sound energy propagates generally back toward the source, or greater than 90 degrees from the primary propagation direction. This type of energy propagation is excluded in the PE method, with 3D PE models instead assigning backward propagating energy to other components of forward propagation or to dissipation mechanisms.[13,14,25] Of note is the ability of propagating modes to couple into horizontally attenuating

https://doi.org/10.1121/10.0001517

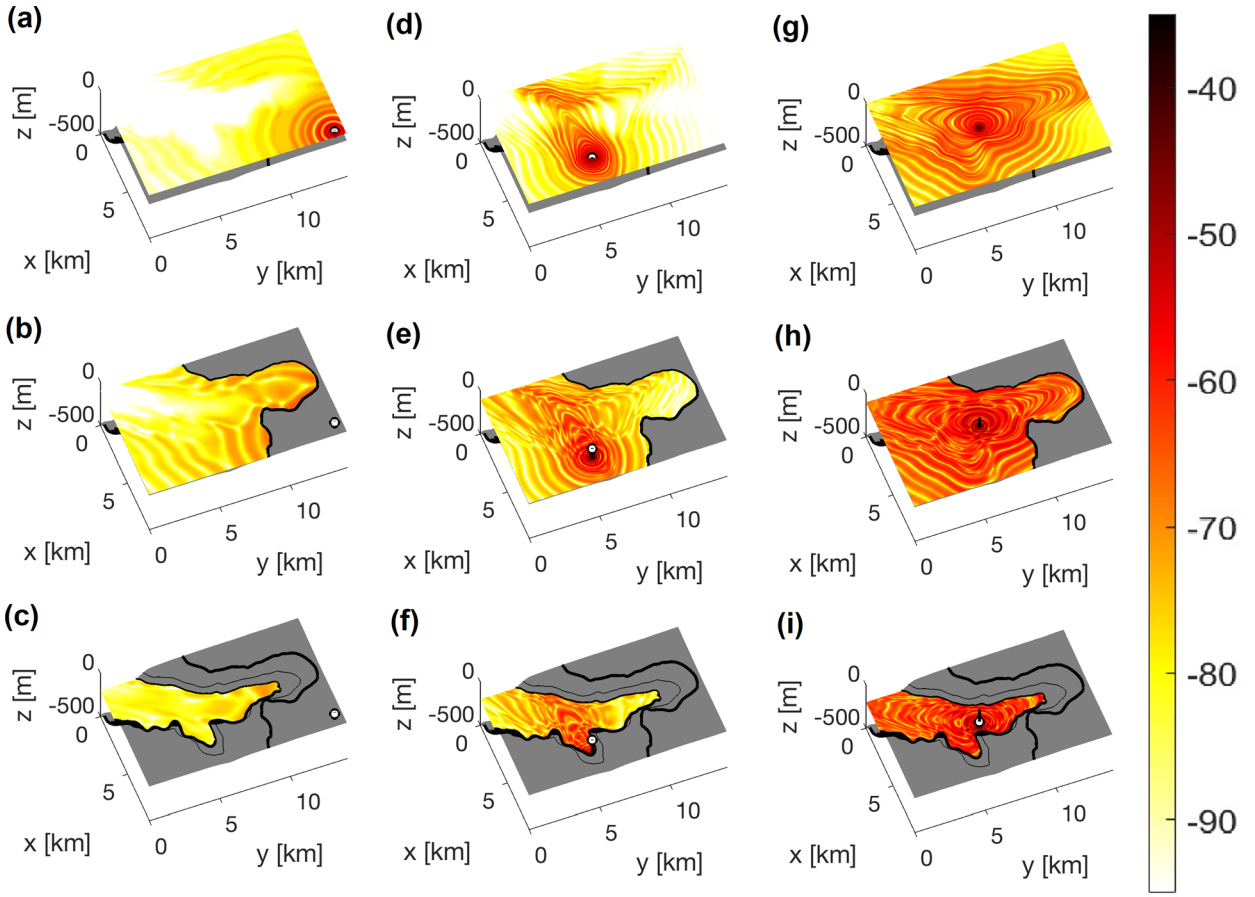

FIG. 7. (Color online) Acoustic intensity. (a)–(c): Source location 1 (S1) is 8 m deep in 89 m of water, with planes at $z = 8$, 100, and 200 m. (d)–(f): Source location 2 (S2) is 8 m deep in 195 m of water, with planes at same depths as (a)–(c). (g)–(i): Source location 3 (S3) is 150 m deep in 297 m of water, with planes at same depths as (a)–(f).

leaky modes to carry modal energy into regions where the adiabatic approximation suggests the leaky modes do not reach. This is most clearly seen in Figs. 8 and 9 where the energy has propagated into the shallow regions of the canyon.

VII. DISCUSSION OF IMPLEMENTATION DIFFICULTIES

The accuracy of the acoustic field solution presented in this paper depends on many factors. The mode functions and modal parameters must be accurate, as well as the coupling coefficients computed from these. These are difficult to know in the real ocean, and determining these in compact areas is the goal of many ocean acoustic inverse experiments. The ability to compute a solution of specified accuracy will also be a function of the number of modes in the model, with computational speed and convergence properties suffering as more modes are used in an effort to improve near-field accuracy. Solutions for environments with easy-to-compute modes, such as uniform hard seabeds, are

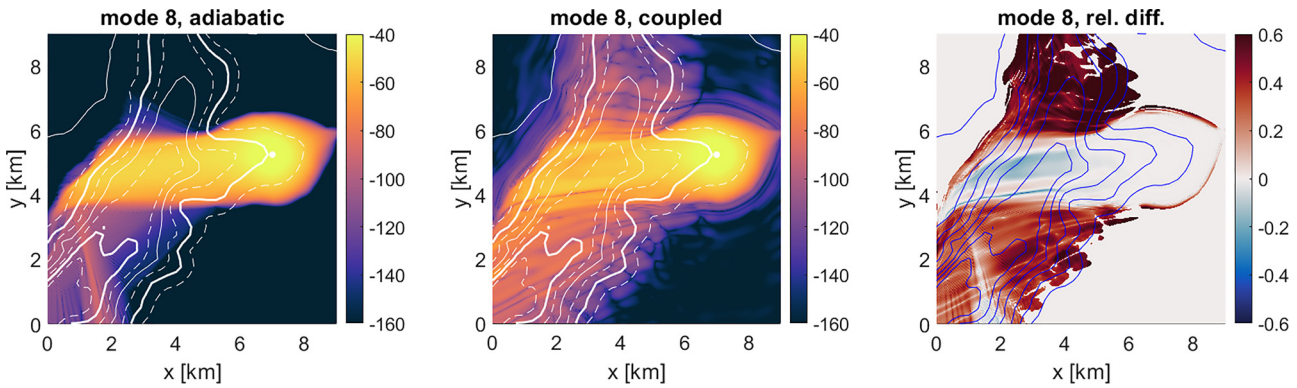

FIG. 8. (Color online) Mode 8 amplitude: adiabatic $10\log_{10}|R_8^{(0)}|^2$, coupled $10\log_{10}|R_8|^2$, and relative difference.

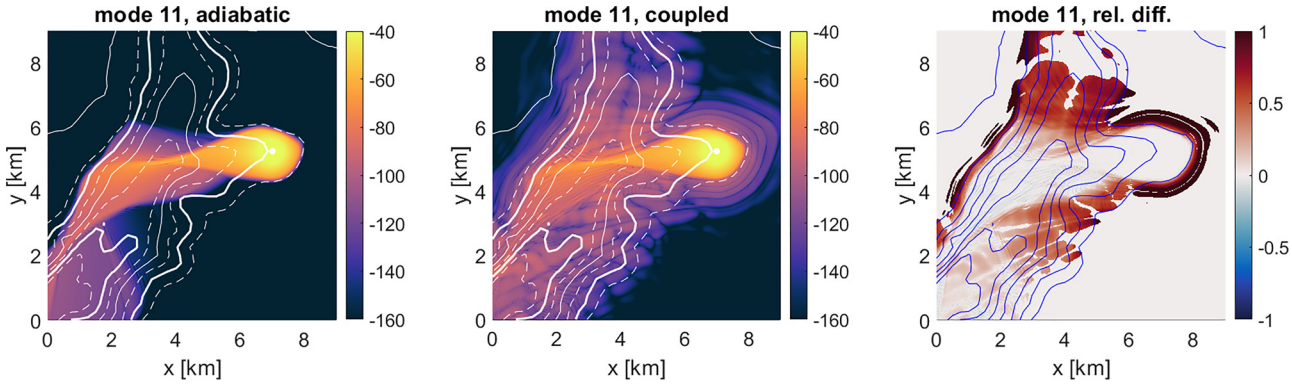

FIG. 9. (Color online) Mode 11 amplitude: adiabatic $10\log_{10}|R_{11}^{(0)}|^2$, coupled $10\log_{10}|R_{11}|^2$, and relative difference.

simpler to compute and verify with the chosen finite-element method, but these are not overly useful for generalized 3D ocean acoustic scenarios.

The general approach taken here is to evaluate the analytically "exact" Helmholtz equation solution in a semi-idealized scenario (fixed sound speed profile, semi-infinite single layer half-space bottom with an attenuation gradient) given by Eq. (1), and introduce only a numerical approximation in the computation process with the exception of the necessary analytical approximation of mode truncation. Without introducing analytical approximations first such as in the PE method, where the directional restriction forces series or rational expansion solutions, implementing the 3D coupled mode model numerically raises a number of complications. Of all the components of the computations, calculating the mode amplitudes given by Eq. (7) is the most challenging. Without approximating the Helmholtz equation as is done in the PE method, a high grid resolution of 10 points per modal horizontal wavelength was required. Even at the long wavelength of about 30 m associated with the 50 Hz source, this leads to millions of spatial points to which the finite element method is applied. To increase efficiency in this coupled mode computation process, this is the portion of the calculation which requires the most attention. In the calculations here, the "backslash" (mldivide) operator in MATLAB is used, which selects one of a number of exact and approximate direct, decomposition, or iterative methods on the matrix equation resulting from the finite element method.[26] One method of speeding up this process is to exchange the computationally expensive sparse matrix inversions with a properly preconditioned iterative approximation process in Eq. (8), which is an area that has seen some research in the underwater acoustics community.[27,28]

A second area of the numerical implementation that adds to the computational complexity is the handling of mode calculations as bathymetry transitions from deep to shallow water. The difficulties stem from two requirements of the method: a sufficient number of modes must be calculated in order to accurately represent the acoustic field, and for all required modes both the mode shape and horizontal modal wavenumber information is needed to compute the mode amplitudes. To determine the number of modes that are needed to represent the acoustic field, higher modes which decay within a short distance of the source location can be discarded. A simple approximation of $1/\mathrm{Im}(k_h) < r_d$ for some selected distance r_d from the source can be used to find modes that attenuate quickly in range to supply a strict lower bound on the number of modes, but with each added mode the number of times that Eq. (8) must be solved increases. This can quickly create an issue when higher frequencies are included and the number of modes increases, and significantly increases the importance of addressing the efficiency of the Helmholtz equation solution method.

Requiring mode and modal wavenumber information everywhere in the horizontal domain is also an issue for generalized environment computations. As the water depth decreases, a mode which may have been trapped in the water can become strongly bottom interacting and no longer integrable as it transitions into the leaky mode domain. In this paper, the issue is addressed by introducing a small gradient in the bottom attenuation and sound speed,[3,19] which will force the modes to decay exponentially after some amplitude growth in the bottom. However, even this approach has its limitations, as the gradient must remain small (suggested[3] less than about 0.18 dB/wavelength and 5.5 m/s/wavelength) to reduce error in the acoustic field in the water. As such, placing a limitation on the size of the gradient restricts the amount of control one has over the depth at which the mode begins to decay exponentially, which in turn can increase the demands on computer hardware as both hard drive and RAM storage requirements increase. This issue arises when a mode which is propagating at the source must travel over a continually decreasing water depth, becoming leakier as it propagates. Of course, leaky modes lose energy into the bottom, so their influence drops off in range. One way to make use of this fact would be to incorporate a method of replacing leaky mode calculations with dummy values that will not introduce meaningful computational errors where the mode influence is negligible. As the mode shapes are also needed for computing coupling coefficients however, implementing this concept is not straightforward, and it was not addressed in this paper.

As a final note to reiterate the importance of increasing the computational efficiency of the Helmholtz

https://doi.org/10.1121/10.0001517

equation solution method, consider that for a problem with N modes that take up to M iterations to converge to an accurate solution, a total of up to NM matrix inversions must be computed. In the numerical tests presented here, $N = 16$, and $M \leq 6$, such that $NM \leq 96$. Including the sponge, the computations presented in this paper were completed on a 3425×5105 grid (which generates a 17.5×10^6 by 17.5×10^6 element sparse matrix), using dual Intel Xeon E5–2680 v4 processors, which each have 14 dual thread cores operating at 2.40 GHz (workstation was built by Pogo Linux, Redmond, WA). For a single sparse matrix inversion which uses MATLAB's multithreading capabilities to compute, the clock time was 6 min and 26 s, while the CPU time was 1 h 34 min 9 s. If a full 6 iterations are required to converge for each mode, which is generally not the case, the clock time for the full computation is more than 10 h, while the CPU time is more than 6 days.

VIII. CONCLUSION

A 3D omnidirectional coupled mode model was presented and implemented numerically in a 9 km × 14 km region of the Hudson Canyon. The environment selected had a bathymetry range from 81 to 494 m of water depth, possessing local slopes of up to 25 degrees or more. To restrict the focus on the influence of bathymetry, a single sound speed profile for the water was replicated throughout the domain and truncated at the water/bottom interface, while three separate source locations in and around the canyon were tested. A comparison between the coupled mode approach and a PE model was given, which revealed differences in acoustic interference patterns in three different horizontal planes. The method described here faces a number of difficulties in implementation which are outlined, and methods for improving efficiency have been discussed. Ultimately, this representation of 3D omnidirectional propagation can be useful for a number of research applications. The 3D mode coupling approach allows for both an analytical and numerical study of the comparative influence of large and small scale bathymetry variations on acoustic fields, and can aid in assessing the reliability of the convenient but physically inaccurate adiabatic approximation. The latter application is of interest, as not only can the adiabatic approximation quite clearly identify complex refractive behavior in a submarine canyon environment as shown in this paper, but it is more readily analyzed via asymptotics to estimate the influence of environmental parameters on acoustic fields.

ACKNOWLEDGMENTS

This work was supported by the Office of Naval Research under a grant to Woods Hole Oceanographic Institution [Grant No. N00014-18-1-2172 which is a Postdoctoral Fellowship for B.J.DeC.]. T.F.D. acknowledges ONR Ocean Acoustics Program Grant No. N00014-17-1-2624.

[1]F. T. Erskine III, *A History of the Acoustics Division of the Naval Research Laboratory: The First Eight Decades 1923–2008* (Naval Research Laboratory, Washington, DC, 2013), p. 38.
[2]C. L. Pekeris, "Theory of propagation of explosive sound in shallow water," Geo. Soc. Am. Mem. **27**, 11–24 (1948).
[3]E. K. Westwood and R. A. Koch, "Elimination of branch cuts from the normal-mode solution using gradient half spaces," J. Acoust. Soc. Am. **106**, 2513–2523 (1999).
[4]M. J. Buckingham and E. M. Giddens, "On the acoustic field in a Pekeris waveguide with attenuation in the bottom half-space," J. Acoust. Soc. Am. **119**, 123–142 (2006).
[5]A. D. Pierce, "Extension of the method of normal modes to sound propagation in an almost-stratified medium," J. Acoust. Soc. Am. **37**, 19–27 (1965).
[6]S. R. Rutherford and K. E. Hawker, "Consistent coupled mode theory of sound propagation for a class of nonseparable problems," J. Acoust. Soc. Am. **70**, 554–564 (1981).
[7]J. A. Fawcett, "A derivation of the differential equations of coupled-mode propagation," J. Acoust. Soc. Am. **92**, 290–295 (1992).
[8]H. J. Lugt and P. Uginčius, "Acoustic rays in an ocean with heat source or thermal-mixing zone," J. Acoust. Soc. Am. **36**, 689–694 (1964).
[9]M. B. Porter, "Beam tracing for two- and three-dimensional problems in ocean acoustics," J. Acoust. Soc. Am. **146**, 2016–2029 (2019).
[10]T. F. Duda, "Initial results from a Cartesian three-dimensional parabolic equation acoustical propagation code," WHOI Technical Report WHOI-2006-14 (Woods Hole Oceanographic Institution, Woods Hole, MA, 2006).
[11]Y.-T. Lin, T. F. Duda, and A. E. Newhall, "Three-dimensional sound propagation models using the parabolic-equation approximation and the split-step Fourier method," J. Comp. Acoust. **21**, 1250018 (2013).
[12]E. K. Westwood, C. T. Tindle, and N. R. Chapman, "A normal mode model for acousto-elastic ocean environments," J. Acoust. Soc. Am. **100**, 3631–3645 (1996).
[13]M. D. Collins and R. B. Evans, "A two-way parabolic equation for acoustic backscattering in the ocean," J. Acoust. Soc. Am. **91**, 1357–1368 (1992).
[14]D. Zhu and L. Bjørnø, "A three-dimensional, two-way, parabolic equation model for acoustic backscattering in a cylindrical coordinate system," J. Acoust. Soc. Am. **108**, 889–898 (2000).
[15]M. S. Ballard and J. D. Sagers, "Measurements and modeling of acoustic propagation in a scale model canyon," J. Acoust. Soc. Am. **146**, 1858–1866 (2019).
[16]F. B. Jensen, W. A. Kuperman, M. B. Porter, and H. Schmidt, *Computational Ocean Acoustics*, 2nd ed. (Springer, New York, 2011), Chaps. 3 and 5.
[17]C. Schär, D. Leuenberger, O. Fuhrer, D. Lüthi, and C. Girard, "A new terrain-following vertical coordinate formulation for atmospheric prediction models," Am. Meteorological Soc. **130**, 2459–2480 (2002).
[18]D. B. Haidvogel, H. Arango, W. P. Budgell, B. D. Cornuelle, E. Curchitser, E. Di Lorenzo, K. Fennel, W. R. Geyer, A. J. Hermann, L. Lanerolle, J. Levin, J. C. McWilliams, A. J. Miller, A. M. Moore, T. M. Powell, A. F. Shchepetkin, C. R. Sherwood, R. P. Signell, J. C. Warner, and J. Wilkin, "Ocean forecasting in terrain-following coordinates: Formulation and skill assessment of the Regional Ocean Modeling System," J. Comp. Phys. **227**, 3595–3624 (2008).
[19]M. S. Ballard, B. M. Goldsberry, and M. J. Isakson, "Normal mode analysis of three-dimensional propagation over a small-slope cosine shaped hill," J. Comp. Acoust. **23**, 155005 (2015).
[20]T. J. R. Hughes, *The Finite Element Method: Linear Static and Dynamic Finite Element Analysis* (Dover Publications, New York, 2000) Chap. 1.
[21]H. K. Brock, "The AESD parabolic equation model," Rep. TN-12, Naval Ocean Research and Development Activity, NSTL Station, MS (1978).
[22]F. Ihlenburg and I. Babuška, "Finite element solution of the Helmholtz equation with high wave number Part I: The h-version of the FEM," Computers Math. Appl. **30**, 9–37 (1995).
[23]M. J. Buckingham, "Array gain of a broadside vertical line array in shallow water," J. Acoust. Soc. Am. **65**, 148–161 (1979).
[24]Y.-T. Lin, K. G. McMahon, J. F. Lynch, and W. L. Siegmann, "Horizontal ducting of sound by curved nonlinear internal gravity

waves in the continental shelf areas," J. Acoust. Soc. Am. **133**, 37–49 (2013).
[25]M. B. Porter, F. B. Jensen, and C. M. Ferla, "The problem of energy conservation in one-way models," J. Acoust. Soc. Am. **89**, 1058–1067 (1991).
[26]*MATLAB: Mathematics*, *2019b* (The MathWorks, Inc., Natick, MA, 2019), pp. 2–14.
[27]E. Larsson and L. Abrahamsson, "Helmholtz and parabolic equation solutions to a benchmark problem in ocean acoustics," J. Acoust. Soc. Am. **113**, 2446–2454 (2003).
[28]N. A. Gumerov and R. Duraiswami, "A broadband fast multipole accelerated boundary element method for the three dimensional Helmholtz equation," J. Acoust. Soc. Am. **125**, 191–205 (2009).